PAPER

Novel dual-network-structured hydrogel microspheres for efficient atmospheric water collection†

Kai Chen, [a] Shijie Han, [a] Shangsheng Zhang, *[a] Hongmei Du,[b] Zhengzhi Zhang,[ac] Jian Wang,[a] Xunkai Luo [a] and Yulian Li[a]

Atmospheric water harvesting (AWH) technology is widely regarded as a promising technology to solve the problem of fresh water shortage. Hygroscopic salt–hydrogel composites have attracted extensive attention due to their high hygroscopic salt-carrying capacity. However, their complex preparation process, salting-out and low water collection efficiency restrict their development. In this study, we prepared calcium alginate (CA) and [2-(methylpropoxy) ethyl dimethyl-(3-propyl sulfonic acid)ammonium hydroxide (PDMAPS)] double-network-structured hydrogel microspheres using a novel drip-free polymerization method. Then, a CA/PDMAPS/CNT/LiCl composite adsorbent was prepared by adding carbon nanotubes (CNTs) and LiCl. The preparation process was simple and suitable for mass production. Zwitterionic groups in the double-network structure (cationic $-N^+(CH_3)_2-$ and anionic $-SO_3^-$) could produce electrostatic effects with Li^+ and Cl^-, thereby binding LiCl and solving the traditional salting-out problem. A binary salt system could also be formed, which greatly enhanced water-collection capacity. At 22 °C with RH = 90%, the maximum water collection of the hydrogel microspheres was 3.586 g g^{-1}. Compared with single-network-structured hydrogels, the reported system exhibited an enhancement of 434% in its water collection efficiency. Under natural light, it desorbed more than 80% of the adsorbed water in 3–4 h. In summary, the dual-network-structured hydrogel microspheres represent a promising material for atmospheric water collection.

1. Introduction

Water is the source of life, upon which all biological processes are essentially dependent. According to the latest report from the World Meteorological Organization (WMO), the shortage of freshwater resources has become one of the most serious challenges facing humanity today. Although there is an abundance of water on the Earth, only 2.8% of the water supply is usable fresh water.[1–3] In recent years, climate change has exacerbated the uneven distribution of water resources, especially in arid and semi-arid regions, where freshwater shortages are increasing, severely affecting human activities and agricultural productivity.[4–6] It is estimated that by 2025, two-thirds of the global population will face a shortage of fresh water.[7,8] To address this pressing issue, researchers have developed various methods to increase freshwater supplies, such as desalination,[9] wastewater recycling,[10] and atmospheric water harvesting (AWH).[11] According to research, there are about 12.9 billion tons of water in the atmosphere in the form of vapour and droplets, which represents an important untapped resource.[12,13] Therefore, how to effectively use this resource has become a research hotspot.

The core components of AWH are water molecular adsorbents.[14,15] The common sorbents are divided into chemical and physical types according to their adsorption mechanism. Chemisorbed materials, such as LiCl, $CaCl_2$ and $MgCl_2$, are widely used because of their high water vapor adsorption capacity, but their regeneration capacity is poor and secondary treatment is difficult.[16,17] Moreover, the adsorption efficiency of physical adsorbents, such as silica gels, activated carbon and zeolite, is low, and there are difficulties in their practical application. Therefore, in order to improve the water collection performance of porous materials, hygroscopic salts such as carbon nanospheres,[18] activated carbon fibres,[19] silica gels, zeolites,[20,21] and metal–organic frameworks (MOFs)[22–24] are embedded in them, but their limited pore volumes hinder their performance. Hydrogels are promising carriers of hygroscopic salts because of their large pore sizes and excellent water-release properties. In particular, materials such as polyacrylamide (PAM) and polyisopropionamide (PNIPAM) hydrogels have

School of Mechanical and Electrical Engineering, China University of Mining and Technology (Beijing), 100083, Beijing, China. E-mail: upzhang2022@163.com

School of Chemical and Environmental Engineering, China University of Mining and Technology (Beijing), 100083, Beijing, China

Asia Pacific Academy of Materials (APAM), Shenyang, 110016, China

demonstrated effective water-harvesting capabilities. However, their practical application is limited by their low salt load capacity, salting-out and difficulties in desorption.[25–27] In recent years, suspension network hydrogels were prepared by freezing gel method, or some special additives were added to change the internal structure and crosslinking density of hydrogels, which increased the salt load of hydrogels. Researchers have used freeze-drying, vacuum-drying and other methods to optimize the internal structure of hydrogels to reduce salt leakage,[28–30] but these still cannot provide an effective solution to the salt leakage problem. Wu[31] et al. prepared a single-network zwitterionic polymer hydrogel (PDMAPS/CNT/LiCl) to solve the salting-out and salt-accumulation problems using cations and ions in hygroscopic salts, but the hygroscopic efficiency was low. Alginate gels are a promising material for atmospheric water collection considering their large specific surface areas and abundant active sites, but they have some drawbacks such as low salt-carrying capacity, salting-out and low moisture-absorption efficiency.[32,33] Wang et al. prepared Bian/FCNT single-network hydrogel composites and constructed a binary salt system for the first time, which greatly enhanced the water-collection performance of the composite adsorbents. However, the problems of salting-out and salt polymerization have still not been systematically solved. Samar[34] et al. prepared a hybrid composite of sodium alginate and SAPO-34, which demonstrated excellent water-collection properties, but the salting-out problem was not solved, and the preparation process was complex and difficult to apply in practice. In summary, the dual-network system constructed by us not only solves traditional problems such as salting-out and salt accumulation but also improve water-collection efficiency through construction of a dual-salt system.

According to the different compositions of dual-network hydrogels, they can be divided into two categories: organic–organic and organic–inorganic hydrogels. Gong[35] et al. prepared a double-network hydrogel composed of a polyacrylamide–acrylic acid copolymer (PAM-co-PAA) and polyvinyl alcohol (PVA) using a simple two-step copolymerization and freezing/thawing method. Sodium alginate (SA) is a natural macromolecule that is commonly used in synthetic hydrogels. Na^+ in the G unit of SA can be ion exchanged with polyvalent metal cations (Zn^{2+}, Fe^{3+}, Ba^{2+}, Cr^{3+}, Ca^{2+}, etc.) in aqueous solutions, such that multiple G units and polyvalent metal cations can be crosslinked to form an "egg box" model. Yu[36] et al. prepared a κ-carrageenan/sodium alginate (κ-car/SA) DN hydrogel using $CaCl_2$ as a crosslinking agent through the calcium hardening method. In this study, SA, PDMAPS, CNTs and a crosslinker (BIS) were blended, and the solution was dropped into $CaCl_2$, initiator (KPS), reducing agent (SDS) and coagulant accelerator (TEMED) solutions by means of dripping to form glues (Fig. S1†). The method has advantages such as simple preparation, low cost and mass production.

Herein, CA/PAMAPS/CNT/LiCl double-network hydrogel microspheres were prepared using a novel drip-free polymerization method. In this double-network structure, there are zwitterionic groups ($-N^+(CH_3)_2^-$ cations and $-SO_3^-$ anions), which can produce electrostatic interactions with Li^+ and Cl^-

when there are a lot of water particles in their interior, forming a binding structure to prevent the accumulation and leakage of LiCl. This solves the problem of leakage and the accumulation of traditional hygroscopic salts while greatly improving cycle stability. In addition, $CaCl_2$ in calcium alginate forms a binary hygroscopic salt system with LiCl bound in the PDMAPS chain, which enhances its water-collection performance.[37] Compared with single-network-structured hydrogels, the water-collection efficiency of our system was increased by 434%. The addition of carbon nanotubes allowed them to desorb water under natural light, thereby requiring no additional energy. Experiments showed that even under low-humidity conditions (RH = 30%), the maximum water-collection rate of our hydrogel microspheres was 1.132 g g^{-1}. Outdoor experiments showed that 5 g of the hydrogel microspheres could collect 8.5 g of fresh water (average humidity of about 60%, average temperature of about 19 °C), with the collected fresh water meeting the international drinking water standards, indicating it was safe to drink. In summary, the dual-network hydrogel microspheres reported in this paper have advantages such as a simple preparation process, no salting-out and a high water-collection efficiency. Therefore, we believe that this material is a promising material for atmospheric water collection.

2. Experimental section

Details on the materials and their sources as well as experimental procedures can be found in ESI.†

3. Results and discussion

3.1 Preparation of the hydrogel microsphere composite material

CA/PDMAPS/CNT hydrogel microspheres were prepared using the drip-free polymerization method and then loaded with LiCl (Fig. 1). In the process of preparing the hydrogel microspheres, SO_4^{2-} was produced through a free polymerization process, which can form $CaSO_4$ insoluble salts in Ca^{2+}, thus affecting the preparation of the hydrogel microspheres. Therefore, the $CaCl_2$ solution used in this experiment had a low concentration. As shown in Table S1,† CA/PDMAPS/CNT hydrogel microspheres with different ratios were prepared by adjusting the proportions of SA and DMAPS monomers. It is worth noting that, as shown in Fig. S2,† PDMAPS hydrogels tended to form on the surface of the microspheres when the mass ratio of SA : DMAPS was lower than 1 : 6. This is because the calcium alginate hydrogel skeleton was not sufficiently developed, making it unable to effectively wrap the PDMAPS network. On the contrary, when the SA content was too high, the load capacity of hygroscopic salts decreased significantly (Fig. S3†). Similarly, we conducted atmospheric water-collection experiments at different ratios and found that the water-collection performance was the best when the mass ratio of SA : DMAPS was 1 : 6 (Fig. S4†); therefore, the mass ratio of SA : DMAPS was 1 : 6 for the sample preparation in the further experiments. Hygroscopic salts were loaded into the hydrogel microspheres by soaking the hydrogels in a saturated hygroscopic salt solution. As shown in Fig. S5,†
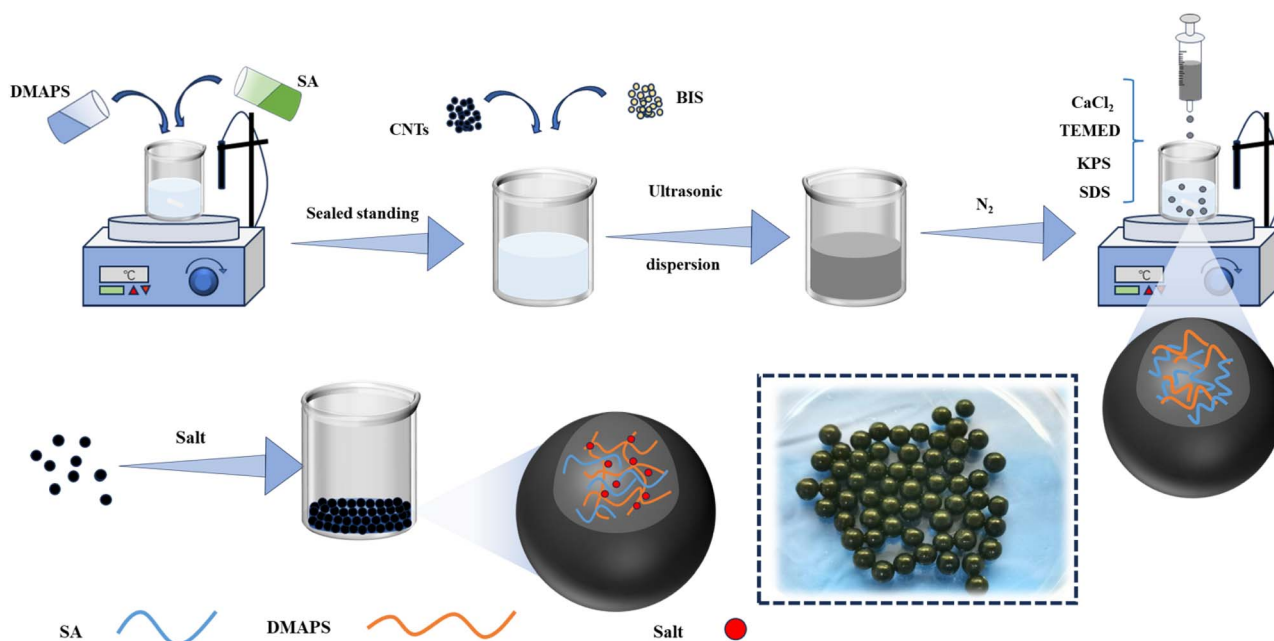
Fig. 1 Schematic of CA/PDMAPS/CNT/salt composite synthesis.

when the CA/CNT/LiCl and CA/PDMAPS/CNT/LiCl hydrogel microspheres were subjected to the same drying conditions, it was obvious that the salt-loading capacity of the CA/CNT hydrogel microspheres was very small, and hygroscopic salts accumulated on the surface after drying, resulting in hygroscopic salt leakage. In contrast, the CA/PDMAPS/CNT composite gels exhibited an excellent salt-carrying calcium capacity without leakage.

3.2 Material morphology and chemical composition

Scanning electron microscopy (SEM) was used to observe surface morphology of the microspheres (Fig. 2d). SEM images showed that the surface of the microspheres had a dense, multilayer irregular macroporous structure. During adsorption and desorption, these pore structures facilitate the transport of water molecules and the escape of water vapor. To verify the formation of the dual-network structure, as shown in Fig. 2e, energy spectrum (EDS) element mapping was performed and showed that the C, Ca and S elements were evenly distributed, confirming the successful formation of the dual-network structure. The hydrogel microspheres were further characterized through Fourier transform infrared (FTIR) spectroscopy (Fig. 2b). In the FTIR spectra of CA/PDMAPS/CNT/LiCl and CA/CNT/LiCl, the characteristic peaks observed at ≈1182 and 1033 cm^{-1} corresponded to the symmetric and asymmetric stretching vibrations of S=O, while the characteristic peak at 1730 cm^{-1} corresponded to the stretching vibrations of C=O.[38] In addition, the peak at 1480 cm^{-1} was correlated to the C–H stretching vibration of the –N$^+$(CH$_3$)$_2$– group. However, there was no S=O peak observed in the FTIR spectra of CA/CNT/LiCl, indicating that the CA/PDMAPS/CNT/LiCl dual-network hydrogels had been successfully synthesized. In addition, the FTIR

spectra of CA/PDMAPS/CNT/LiCl and CA/CNT/LiCl showed wide water absorption peaks in the regions of 3000–3700 and 3400–3600 cm^{-1}, respectively, confirming the presence of hygroscopic salts and their water absorption during the tests. Moreover, the water peak of the CA/PDMAPS/CNT/LiCl hydrogel microspheres was wider, indicating that PDMAPS effectively improved the salt-carrying capacity, thus promoting greater water adsorption.

3.3 Formation of a binary salt system

As shown in Fig. 3a, zwitterionic polymers (DMAPS) contain –N$^+$(CH$_3$)$_2$– (cation) and –SO$_3$$^-$ (anion) groups. The electrostatic interactions between the anion and cationic groups led to the self-association of the PDMAPS polymerization chains, resulting in the super-dense structure of the PDMAPS hydrogels, which became opaque. However, when a LiCl aqueous solution was added to the PDMAPS hydrogels, the PDMAPS hydrogels gradually became transparent. This is because Li$^+$ and Cl$^-$ have an electrostatic interaction with the anionic groups on the PDMAPS chain, prompting it to open and thus become transparent.

The formation of a binary salt system is a complicated process. First, Na$^+$ in the G-block of sodium alginate is replaced by Ca^{2+}, forming a calcium alginate hydrogel (CA) that resembles an "eggshell" structure. The dual-network architecture built by us is shown in Fig. 3b. First, CaCl$_2$ was present in the preparation process; therefore, the zwitterionic groups on the PDMAPS chain could bind Ca^{2+} with Cl$^-$. In high-concentration LiCl solution, the Na$^+$ in the calcium alginate G-block was also replaced by Li$^+$. The bound part of the PDMAPS chain Ca^{2+} was replaced by Li$^+$, and a binary salt system was formed. Interestingly, we impregnated CA/PDMPAS hydrogel microspheres with deionized water, removed internal CaCl$_2$, and then placed them

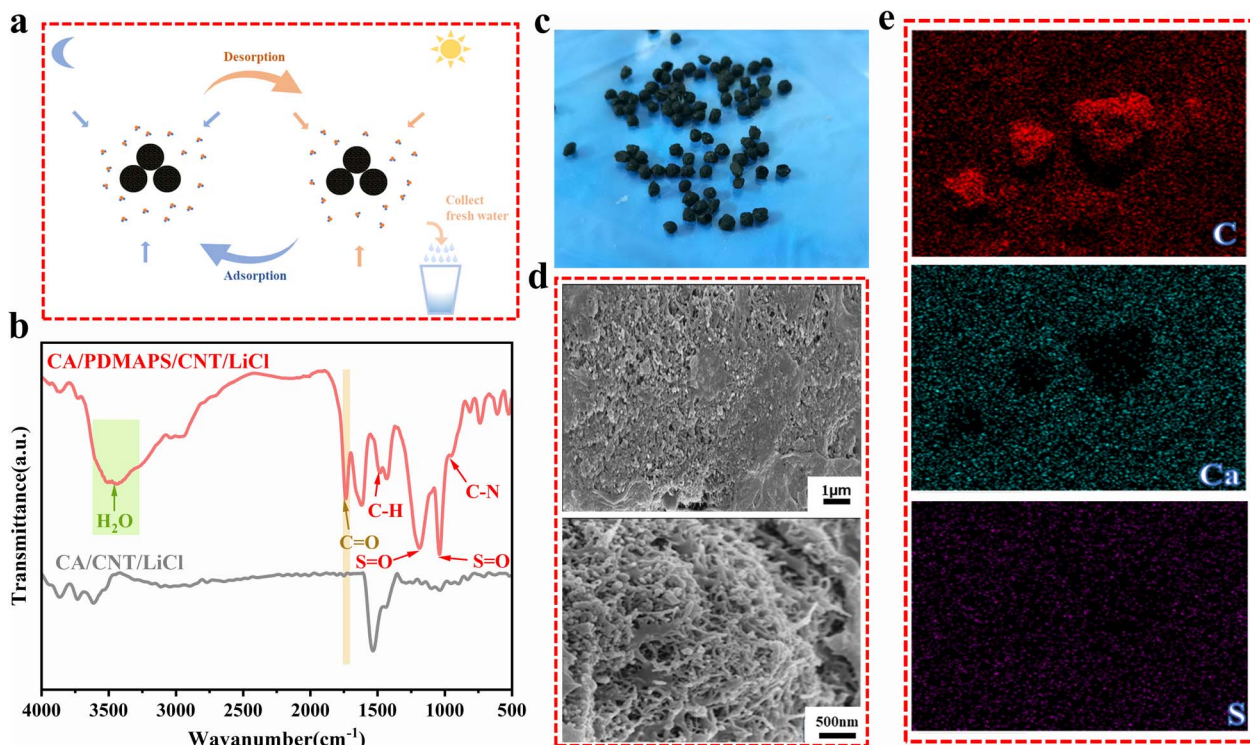© 2025 The Author(s). Published by the Royal Society of Chemistry

Fig. 2 (a) Schematic of the CA/PDMAPS/CNT/LiCl hydrogels for atmospheric water harvesting. (b) FTIR spectra of the CA/PDMAPS/CNT/LiCl and CA/CNT/LiCl hydrogels. (c) Optical photo of the CA/PDMAPS/CNT/LiCl hydrogel microspheres. (d) SEM images of the CA/PDMAPS/CNT/LiCl hydrogel microspheres. (e) Element mapping of the CA/PDMAPS/CNT/LiCl hydrogels.

in LiCl aqueous solutions of different concentrations. As shown in Fig. S6,† Li^+ could replace a small amount of Ca^{2+}, and this phenomenon occurred more and more with the increase in the salt solutions.

3.4 Swelling capacity of the CA/PDMAPS/CNT/LiCl hydrogels

The effect of salt concentration on the expansion capacity of the hydrogel microspheres was investigated using an immersion
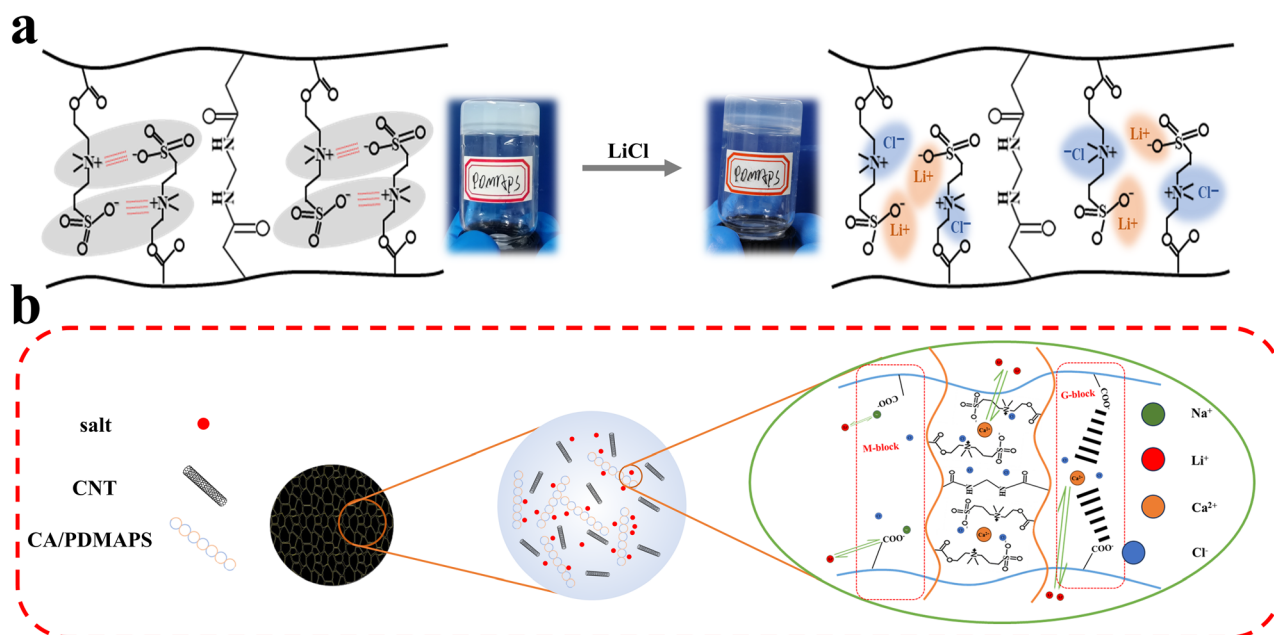

Fig. 3 LiCl binding mechanism and formation diagram of the binary hygroscopic salt system. (a) PDMAPS hydrogel structure and PDMAPS/LiCl structure diagram. (b) CA/PDMAPS/CNT/LiCl hydrogel structure diagram.

method. The CA/PDMAPS/CNT, CA/CNT and PDMAPS/CNT hydrogel microspheres were immersed in LiCl solutions of different concentrations for 12 h. As shown in Fig. 4a, the swelling ratios of the CA/PDMAPS/CNT, CA/CNT and PDMAPS/CNT hydrogels increased with an increase in LiCl solution concentration, especially the performance of the CA/PDMAPS/CNT and PDMAPS/CNT hydrogels. When the LiCl concentration was 0.1 g mL^{-1}, the swelling rations reached 12.134 g g^{-1}, 5.5 g g^{-1} and 10.568 g g^{-1}. Owing to the presence of $-N^+(CH_3)_2{}^-$ and $-SO_3{}^-$ zwitterionic groups in the CA/PDMAPS/CNT and PDMAPS/CNT hydrogels, the swelling ratio of deionized water was low because of self-association. With the entry of LiCl, the self-association structure was broken and the swelling ratio increased. In addition, as part of the Ca^{2+} in CA/PDMAPS/CNTs was replaced by Li$^+$,[39] the swelling ratio further increased. The swelling ratio of the CA/CNT hydrogels also increased when part of the Ca^{2+} was replaced by Li$^+$. Interestingly, we immersed the CA/CNT and CA/PDMAPS/CNT hydrogels in a low-concentration LiCl solution. As shown in Fig. 4b, the swelling ratio of the CA/CNT hydrogels was higher when the LiCl concentration was low, because Li$^+$ replaced Ca^{2+} at this time. The swelling ratios of the CA/CNT and CA/PDMAPS/CNT hydrogels decreased with an increasing LiCl concentration. On the one hand, Li$^+$ and Cl$^-$ shield $-COO^-$ on the calcium alginate polymer chains, resulting in weaker repulsion among these chains and a lower swelling ratio. On the other hand, Li$^+$ and Cl$^-$ are conducive to breaking

the self-association of $-N^+(CH_3)_2{}^-$ and $-SO_3{}^-$ on the PDMAPS polymer chain, which increases the swelling ratio. Therefore, combining all these factors, we believe that CA/PDMAPS/CNTs had a stronger salt tolerance and could enable a higher LiCl loading than CA/CNTs. With the increasing LiCl concentration, although the swelling ratio of the CA/PDMAPS/CNT and PDMAPS/CNT hydrogels decreased, the swelling ratio was still higher than that of pure water. The CA/PDMAPS/CNT and PDMAPS/CNT hydrogels were compatible with more LiCl, which was conducive to atmospheric water collection. As shown in Fig. 4c, the water vapor adsorption isotherms of the CA/PDMAPS/CNT/LiCl hydrogels were measured at 22 °C. At RH = 90%, the hydrogel microspheres collected 3.586 g g^{-1} water in 6 h, demonstrating an extremely high water-collection capacity. The water vapor adsorption isotherm of the CA/PDMAPS/CNT/LiCl hydrogel is shown in Fig. 4d. The curve did not show any saturation point, indicating the large density and large pore structure inside the material. The water-collection process of hydrogel microspheres can be divided into two processes: surface trapping of water molecules and salt solution transfer to the gel interior. First, LiCl on the surface of the gels captures water molecules in the air to form a salt solution, and the time required for this process decreases with the increase in relative humidity. The salt solution formed on the surface is then transferred to the inside of the gels through their pores based on their size.[40] According to Smith's hypothesis,[41] the hydrogel
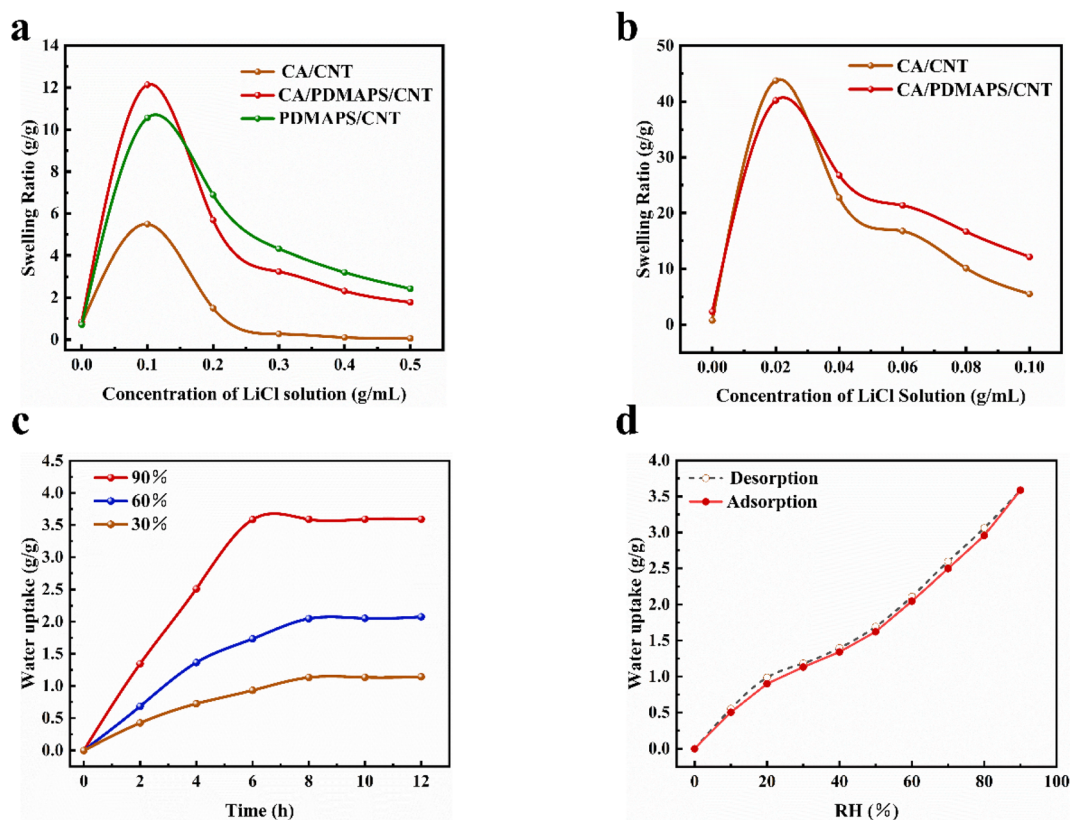

Fig. 4 (a) Swelling ratios of the CA/CNT, CA/PDMAPS/CNT and PDMAPS/CNT hydrogels in LiCl aqueous solutions with different concentrations. (b) Swelling ratio of the CA/CNT and CA/PDMAPS/CNT hydrogels in LiCl solution with lower concentrations. (c) Moisture absorption properties of the CA/PDMAPS/CNT hydrogels at RH = 30%, 60% and 90%. (d) Water vapor sorption isotherms of CA/PDMAPS/CNT/LiCl at 22 °C.

microsphere isotherm can be divided into two parts. The first part mainly involves the formation of an aqueous solution of water molecules on the surface of the microspheres (corresponding to the convex part of the curve with an RH between 0 and 40%), which was mainly determined by the relative humidity. In the second part, water molecules are transferred into the internal structure of the polymers, resulting in a concave curvature (RH above 40%). This is because when the relative humidity was less than 40%, water vapor could not effectively diffuse into the internal structure, so the relative humidity increased, and the amount of water vapor absorbed gradually increased. When the relative humidity was greater than 40%, the hydrophilic gel matrix was closely linked, and the capillary action could act as a driving force for rapid water transport, resulting in a sharper rise in the water-vapor-absorption capacity. At the same time, at RH = 60% and 30%, the water collection capacities of the hydrogel microspheres in 8 h were 2.047 and 1.132 g g^{-1}, respectively. The results show that the prepared double-mesh hydrogel microspheres had a higher and faster water collection capacity under both low and high humidity conditions. Therefore, we consider them to be promising materials for atmospheric water harvesting.

3.5 Adsorption and desorption capacity and photothermal characteristics

Because the size and shape of an adsorbent have an effect on its adsorption performance, in order to more intuitively evaluate their water-collecting performance, we prepare samples of the same size and shape as much as possible. The water-collecting properties of the CA/PDMAPS/CNT/LiCl, CA/CNT/LiCl and

PDMAPS/CNT/LiCl hydrogels were then evaluated under different relative humidity conditions (relative humidities of 30%, 60% and 90%, respectively) at 22 °C. As shown in Fig. 5a, once the relative humidity started to rise above 0%, all the samples begin to adsorb water vapor. The water vapor adsorption capacity increased with the increase in relative humidity. Among them, CA/PDMAPS/CNT/LiCl demonstrated the best water collection performance. Especially under the condition of a high relative humidity, the water-collection performance of the CA/PDMAPS/CNT/LiCl hydrogel microspheres was significantly enhanced with the increase in relative humidity, indicating that the dual-network-structured binary salt system we constructed was conducive to improving the water-collection performance. Compared with CA/CNT/LiCl and PDMAPS/CNT/LiCl single-network-structured hydrogels, the water-collection efficiencies were increased by 434% and 86%, respectively. Subsequently, we evaluated the water vapor adsorption kinetics of the CA/PDMAPS/CNT/LiCl, CA/CNT/LiCl and PDMAPS/CNT/LiCl hydrogels using a static RH test at 22 °C and RH = 90%. As shown in Fig. 5b, CA/PDMAPS/CNT/LiCl reached catchment saturation within 6 h. After desorption at 75 °C, CA/PDMAPS/CNT/LiCl could release almost all the adsorbed water within 2 h. However, a small amount of adsorbed water remained inside the gels in the form of salt crystal water. The results from the thermogravimetric analysis (Fig. 5c) showed that as the temperature continued to rise, the salt crystal water inside the hydrogels was continuously lost, and did not participate in the adsorption or desorption cycles.[42] The CA/PDMAPS polymer structure of CA/PDMAPS/CNT/LiCl began to degrade at about
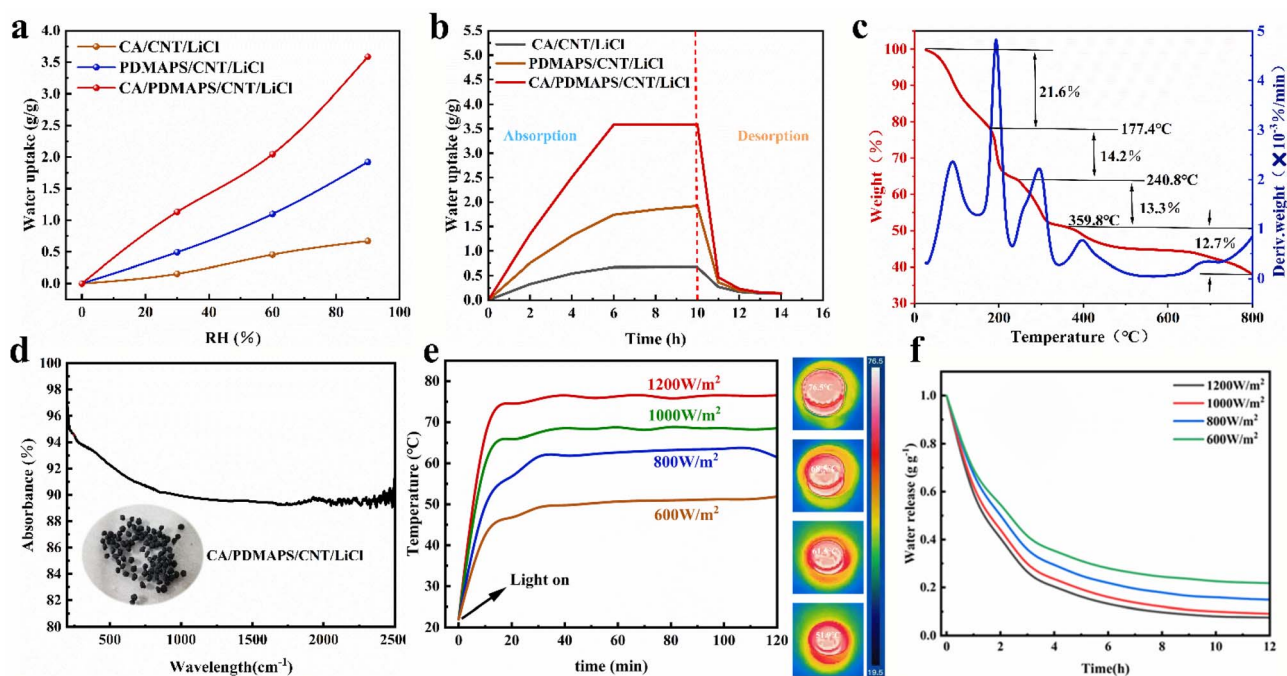

Fig. 5 (a) Water sorption isotherms at 22 °C. (b) Static water absorption–desorption curves. (c) CA/PDMAPS/CNT/LiCl hydrogel TGA curve and (d) UV–vis–NIR absorption spectrum. (e) CAPDMAPS/CNT/LiCl hydrogel surface temperature change with time and infrared thermal image at different light intensities. (f) Water desorption at different light intensities.

240 °C, which was much higher than the desorption temperature, indicating its excellent thermal stability.

To explore the photothermal properties of the CA/PDMAPS/CNT/LiCl hydrogels, UV–vis–NIR tests were performed (Fig. 5d). Owing to the photothermal properties of carbon nanotubes, the CA/PDMAPS/CNT/LiCl hydrogels had a high absorption spectrum over the entire sunlight range, with an average absorption rate of about 92%. We further investigated the photothermal properties of the CA/PDMAPS/CNT/LiCl hydrogels using different light intensities (600, 800, 1000 and 1200 W m^{-2}). First, we tested the dried hydrogel microspheres in a Petri dish at room temperature. As shown in Fig. 5e, in about 20 min, the surface temperature of the hydrogels reached 46.8 °C, 56.8 °C, 65.9 °C and 74.5 °C, respectively. In summary, the CA/PDMAPS/CNT/LiCl hydrogels demonstrated excellent photothermal properties. Next, the solar desorption performance of the CA/PDMAPS/CNT/LiCl hydrogels was tested at different light intensities. A CA/PDMAPS/CNT/LiCl hydrogel containing approximately 1 g g^{-1} of adsorbed water was exposed to simulated sunlight. As shown in Fig. 5f, more than 80% of the adsorbed water was released within 3–4 h. As the content of adsorbed water decreased, the release rate slowed

down. The higher the light intensity, the greater the release of adsorbed water. These experimental results confirmed the desorption feasibility of the CA/PDMAPS/CNT/LiCl hydrogels under natural light.

3.6 AWH of the CA/PDMAPS/CNT/LiCl hydrogel

The atmospheric water collection (AWH) process includes water vapor adsorption at night, solar-driven desorption during the day, and the condensation and collection of water. The outdoor water collection experiment is shown in Fig. 6a. About 5 g of hydrogel samples was placed in a Petri dish and exposed to an outdoor environment for water adsorption overnight. As shown in Fig. 6b, the average temperature during the experiment was 19 °C and the average relative humidity was 55%. After 11 h of adsorption, about 12.7 g of adsorbed water was collected. The high adsorption efficiency of the hydrogels under these conditions was thus proven.

For the desorption process, the samples were transferred to a laboratory-made device consisting of a sealed plastic housing (Fig. 6c). As shown in Fig. 6d, the CA/PDMAPS/CNT/LiCl hydrogels began desorbing water upon solar radiation. Water vapor condensed on the inner surface of the plastic shell to
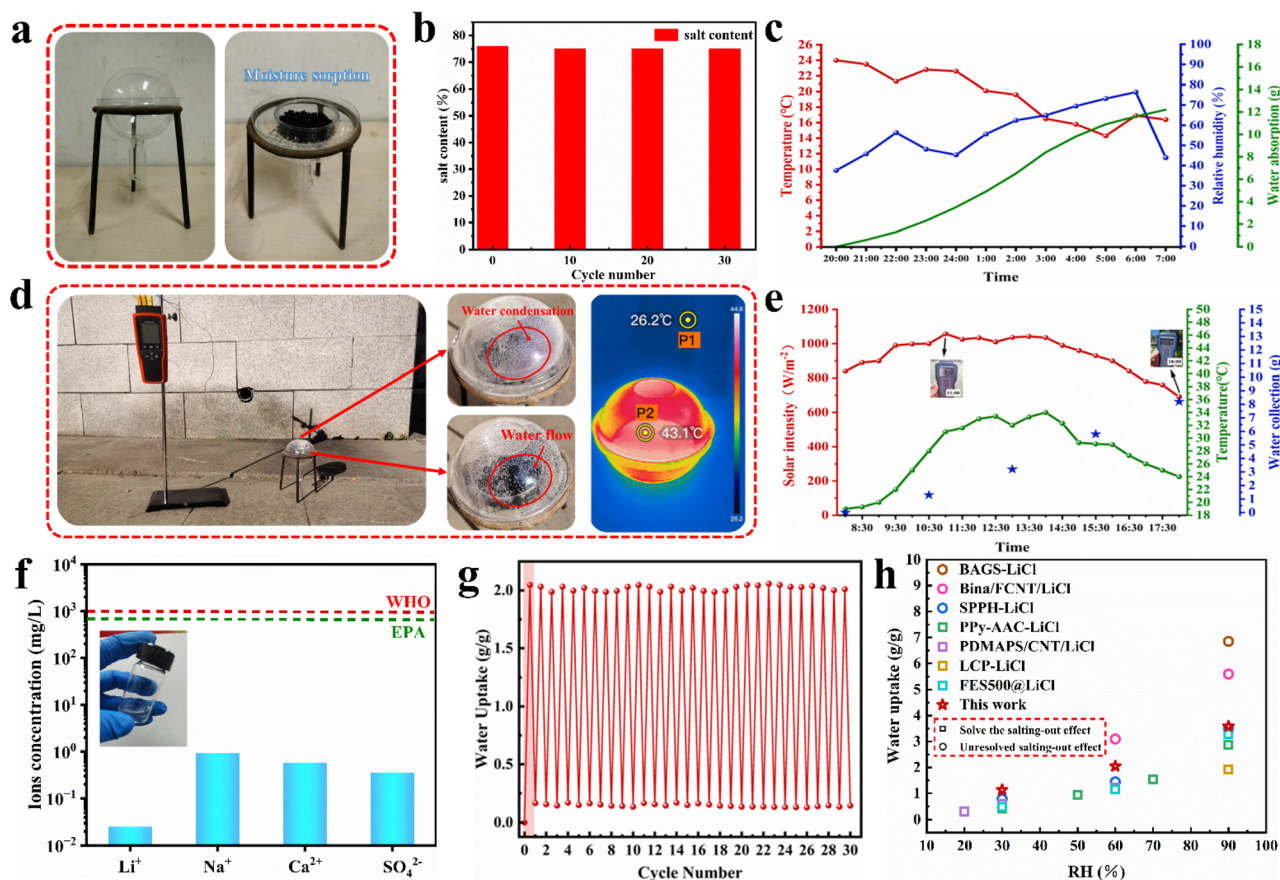

Fig. 6 Outdoor water harvesting experiment. (a) Diagram of the atmospheric water collection device. (b) Salt content of the CA/PDMAPS/CNT/LiCl hydrogels after multiple cycles. (c) Temperature, humidity, and water uptake of the hydrogels at night. (d) Formation of water droplets in the inner wall of the device and infrared thermal imaging performed under natural light irradiation. (e) Light intensity and mass change of collected water during the day. (f) Collected water and corresponding ion concentrations. (g) CA/PDMAPS/CNT/LiCl hydrogel cycle stability test. (h) Comparison of this study with other studies.

Paper

form droplets, and when the droplets grew large enough, they flew along the circular container into the bottom collection chamber. As shown in Fig. 6e, since the beginning of the experiment, the solar light intensity gradually increased, reaching a peak value of 1056.7 W m^{-2} at around 11 am, thereby dropping to a minimum value of 691 W m^{-2} after 6 pm. During this period, *i.e.*, after 10 h of sunlight, about 8.5 g of fresh water was collected. During the cyclic desorption process, only $\approx 64\%$ of the adsorbed water was collected, which was mainly owing to the presence of residual adsorbed water in the hydrogels and the partial release of water adhering to the container wall, hindering full recovery. In addition, we collected fresh water for ion detection. As shown in Fig. 6f, the ion concentrations in the collected water (Li^+, Na^+, Ca^{2+}, and SO_4^{2-}) were measured and found to be well below the standards set by the WHO and the U.S. EPA Drinking Water Standards. These results confirm that the water collected from the atmosphere using the CA/PDMAPS/CNT/LiCl hydrogel microspheres was safe and clean for use in everyday life.

We also evaluated the cycling properties of the CA/PDMAPS/CNT/LiCl hydrogels. As shown in Fig. 6g, the CA/PDMAPS/CNT/LiCl hydrogels were first adsorbed at 22 °C and RH = 60% for 8 h and then desorbed at 70 °C and RH = 0%. This cycle was repeated 30 times. After 30 cycles, the CA/PDMAPS/CNT/LiCl hydrogels still had a high adsorption capacity, showing their high cyclic stability. We next evaluated whether the CA/PDMAPS/CNT/LiCl hydrogels could prevent salting-out. As shown in Fig. 6b, the salt content of the hydrogel microspheres before the cycling experiment was 76%, and the salt content remained unchanged at about 75% after 30 cycles. We placed the CA/CNT and CA/PDMAPS/CNT/LiCl hydrogels on copper plates at 22 °C and RH = 60%. As shown in Fig. S7,† after 14 days, the copper plate placed with the CA/PDMAPS/CNT/LiCl hydrogels was not corroded, while that placed with the CA/CNT hydrogel was corroded. This indicated that the CA/PDMAPS/CNT/LiCl hydrogels had no LiCl leakage. We compared the experimental results with those of previous studies. As shown in Fig. 6h, we compared the performance with that of hygroscopic saline gel composite adsorbents in recent years. It was confirmed that the CA/PDMAPS/CNT/LiCl hydrogels prepared by us had excellent water-collection performance and could solve the salting-out effect.[43-48]

4. Conclusions

In summary, we prepared double-network hydrogel microspheres using a novel drip-free polymerization method, which is simple, cost-effective and can be produced in large quantities. This dual-network system could not only solve the problem of traditional salting-out but also form a binary salt system with a greatly enhanced water-collection performance. We verified that the CA/PDMAPS/CNT/LiCl hydrogels had a high water-vapor-adsorption capacity, strong water-storage capacity and stability through water collection experiments. At 22 °C, with RH = 30%, 60% and 90%, the water-collection rates were 1.132, 2.047 and 3.586 g g^{-1}, respectively. Compared with single-network hydrogels, the water collection performance was

improved by 434%. Under natural light, the hydrogel desorbed more than 80% of the absorbed water in 3–4 h. After 30 sorption–desorption cycles, the hygroscopic properties of the products did not decrease significantly. We designed an outdoor atmospheric water collection device and collected 8.5 g of fresh water in one day and one night with 5 g of samples, and the fresh water produced met international drinking water standards. Outdoor experiments also successfully demonstrated the hydrogels' ability to produce fresh water from the atmosphere, indicating that they are promising atmospheric water-collection materials. This study successfully prepared atmospheric water collection materials through a simple-process, with a non-hygroscopic salting-out and efficient water collection performance, that have potential as a sustainable solution to solve the problem of freshwater shortages.

Data availability

The data are available from the corresponding author upon reasonable request.

Author contributions

Kai Chen, Shangsheng Zhang, Shijie Han and Hongmei Du designed and performed the experiments, analysed the data, and wrote the original draft; Xunkai Luo, Jian Wang and Yulian Li conducted the characterization experiments; Zengzhi Zhang supervised the work; and all the authors reviewed and edited the manuscript.

Conflicts of interest

The authors declare that they have no known competing financial interests or personal relationships that could have appeared to influence the work reported in this paper.

Acknowledgements

Notes and references

1 Q. Li, Y. Ying, Y. Tao and H. Li, *Ind. Eng. Chem. Res.*, 2022, **61**, 1344–1354.

2 W. Wang, Y. Shi, C. Zhang, S. Hong, L. Shi, J. Chang, R. Li, Y. Jin, C. Ong, S. Zhuo and P. Wang, *Nat. Commun.*, 2019, **10**, 3012.

3 D. Zhan and Z. Guo, *Mater. Horiz.*, 2023, **10**, 4827–4856.

4 M. Karimi, M. Tabiee, S. Karami, V. Karimi and E. Karamidehkordi, *Groundw. Sustain. Dev.*, 2024, **24**, 101075.

5 S. Wakekar and C. Das, *Sustainable Mater. Technol.*, 2024, **42**, e01120.

6 S. Zhang, S. Xu, Y. Liu, R. Lei, T. Guo, Y. Yao, S. Gao, J. Ding and Z. Zhang, *Prog. Nat. Sci.:Mater. Int.*, 2023, **33**, 37–46.

7 Z. Ahrestani, S. Sadeghzadeh and H. B. Motejadded Emrooz, *RSC Adv.*, 2023, **13**, 10273–10307.

8 H. Zhu, Z. Guo and W. Liu, *Chem. Commun.*, 2016, **52**, 3863–3879.

9 M. Ayaz, M. A. Namazi, M. A. u. Din, M. I. M. Ershath, A. Mansour and E.-H. M. Aggoune, *Desalination*, 2022, **540**, 116022.

10 H. Wang, J. Xu and L. Sheng, *J. Cleaner Prod.*, 2020, **258**, 120760.

11 D. Nioras, K. Ellinas and E. Gogolides, *ACS Appl. Nano Mater.*, 2022, **5**, 11334–11341.

12 M. Wu, R. Li, Y. Shi, M. Altunkaya, S. Aleid, C. Zhang, W. Wang and P. Wang, *Mater. Horiz.*, 2021, **8**, 1518–1527.

13 X. Zhou, H. Lu, F. Zhao and G. Yu, *ACS Mater. Lett.*, 2020, **2**, 671–684.

14 B. Guo, F. Li, C. Wang, L. Zhang and D. Sun, *J. Mater. Chem. A*, 2019, **7**, 13173–13179.

15 Y. Hu, Z. Fang, X. Ma, X. Wan, S. Wang, S. Fan, Z. Ye and X. Peng, *Appl. Mater. Today*, 2021, **23**, 101076.

16 X. Wang, X. Li, G. Liu, J. Li, X. Hu, N. Xu, W. Zhao, B. Zhu and J. Zhu, *Angew. Chem., Int. Ed.*, 2019, **58**, 12054–12058.

17 N. Yu, R. Z. Wang, Z. S. Lu, L. W. Wang and T. F. Ishugah, *Energy*, 2014, **67**, 468–478.

18 R. Li, Y. Shi, M. Wu, S. Hong and P. Wang, *Nano Energy*, 2020, **67**, 104255.

19 J. Y. Wang, R. Z. Wang and L. W. Wang, *Appl. Therm. Eng.*, 2016, **100**, 893–901.

20 I. V. Ponomarenko, I. S. Glaznev, A. V. Gubar, Y. I. Aristov and S. D. Kirik, *Microporous Mesoporous Mater.*, 2010, **129**, 243–250.

21 S. Zhang, Z. Zhang, K. Chen, S. Xu, X. Luo, Y. Liu, J. Wang, S. Han, Y. Li and H. Du, *Prog. Nat. Sci.:Mater. Int.*, 2024, **34**, 1093–1099.

22 S. Guo, Y. Hu, Z. Fang, B. Yao and X. Peng, *RSC Adv.*, 2024, **14**, 15619–15626.

23 Y. Guo, Y. Ying, Y. Mao, X. Peng and B. Chen, *Angew. Chem., Int. Ed.*, 2016, **55**, 15120–15124.

24 F. Luo, X. Liang, W. Chen, S. Wang, X. Gao, Z. Zhang and Y. Fang, *Chem. Eng. J.*, 2023, **465**, 142891.

25 B. Kang, H. Tang, Z. Zhao and S. Song, *ACS Omega*, 2020, **5**, 6229–6239.

26 C. Lei, Y. Guo, W. Guan, H. Lu, W. Shi and G. Yu, *Angew. Chem., Int. Ed.*, 2022, **61**, e202200271.

27 X. Wang, G. Ma, S. Cui, K. Sun, W. Li and H. Peng, *Small*, 2024, **20**, 2307416.

28 C. Xiang, X. Yang, F. Deng, Z. Chen and R. Wang, *Appl. Phys. Rev.*, 2023, **10**, 041413.

29 X. Yang, Z. Chen, C. Xiang, H. Shan and R. Wang, *Nat. Commun.*, 2024, **15**, 7678.

30 H. Zou, X. Yang, J. Zhu, F. Wang, Z. Zeng, C. Xiang, D. Huang, J. Li and R. Wang, *Angew. Chem.*, 2024, **2**, 663–673.

31 S. Aleid, M. Wu, R. Li, W. Wang, C. Zhang, L. Zhang and P. Wang, *ACS Mater. Lett.*, 2022, **4**, 511–520.

32 D. Zheng, X. Xu, J. Zhu, B. Bai, Q. Wang, W. Shi and J. Li, *J. Environ. Chem. Eng.*, 2023, **11**, 109247.

33 H. Zhou, L. Yan, D. Tang, T. Xu, L. Dai, C. Li, W. Chen and C. Si, *Adv. Mater.*, 2024, **36**, 2470251.

34 S. N. Abd Elwadood, A. S. F. Farinha, Y. Al Wahedi, A. Al Alili, G.-J. Witkamp, L. F. Dumee and G. N. Karanikolos, *Small*, 2024, **20**, 2400420.

35 G. Zhengyu, Z. Guoping, Z. Xiaoliang, L. Jinhui, L. Gang, H. Wangping, S. Rong and W. Chingping, *ACS Appl. Mater. Interfaces*, 2016, **8**, 24030–24037.

36 F. Yu, T. Cui, C. Yang, X. Dai and J. Ma, *Chemosphere*, 2019, **237**, 124417.

37 A. Entezari, M. Ejeian and R. Wang, *ACS Mater. Lett.*, 2020, **2**, 471–477.

38 W. Guo, X. Li, F. Xu, Y. Li and J. Sun, *ACS Appl. Mater. Interfaces*, 2018, **10**, 13073–13081.

39 S. Saitoh, Y. Araki, R. Kon, H. Katsura and M. Taira, *Dent. Mater. J.*, 2000, **19**, 396–404.

40 G. Weixin, Z. Yaxuan, L. Chuxin and Y. Guihua, *Proc. Natl. Acad. Sci. U. S. A.*, 2023, **120**, e2308969120.

41 S. N. A. Elwadood, A. S. F. Farinha, Y. A. Wahedi, A. A. Alili, G. J. Witkamp, L. F. Dumée and G. N. Karanikolos, *Small*, 2024, 2400420.

42 A. K. Bhattacharya, A. Hartridge and K. K. Mallick, *J. Mater. Sci.*, 1997, **32**, 1113–1116.

43 N. Ding, B. Liang, X. Gao, D. Yao, J. Chen, C. Liu, C. Lu and X. Pang, *Chem. Eng. J.*, 2024, **495**, 153470.

44 S. N. A. Elwadood, A. S. F. Farinha, Y. A. Wahedi, A. A. Alili, G. J. Witkamp, L. F. Dumée and G. N. Karanikolos, *Small*, 2024, **20**, e2400420.

45 A. Entezari, M. Ejeian and R. Wang, *ACS Mater. Lett.*, 2020, **2**, 471–477.

46 M. Song, T. Cheng, Y. Li, D. Huang, X. Huang, H. Xie, L. Wang, Y. Yue and W. Yu, *J. Cleaner Prod.*, 2024, **461**, 142661.

47 L. Tong, W. Zhaoyang, L. Ruonan, C. Kun, L. He and T. Ye, *ACS Appl. Mater. Interfaces*, 2022, **14**, 32433–32443.

48 D. Zhan, C. Fu, Z. Yu, G. Tian, Y. He, X. Chen and Z. Guo, *Mater. Today Phys.*, 2025, **51**, 101658.